Flame describing functions of a confined premixed swirled combustor with upstream and downstream forcing

R Gaudron, Marco Gatti, Clément Mirat, Thierry Schuller

Flame Describing Functions of a Confined Premixed Swirled Combustor With Upstream and Downstream Forcing

R. Gaudron
Laboratoire EM2C,
CNRS, CentraleSupélec,
Université Paris-Saclay,
3, rue Joliot Curie,
Gif-sur-Yvette cedex 91192, France

M. Gatti
Laboratoire EM2C,
CNRS, CentraleSupélec,
Université Paris-Saclay,
3, rue Joliot Curie,
Gif-sur-Yvette cedex 91192, France

C. Mirat
Laboratoire EM2C,
CNRS, CentraleSupélec,
Université Paris-Saclay,
3, rue Joliot Curie,
Gif-sur-Yvette cedex 91192, France

T. Schuller
Laboratoire EM2C,
CNRS, CentraleSupélec,
Université Paris-Saclay,
3, rue Joliot Curie,
Gif-sur-Yvette cedex 91192, France;
Institut de Mécanique des Fluides
de Toulouse (IMFT),
Université de Toulouse,
CNRS, INPT, UPS,
2 allée du Professeur Camille Soula,
Toulouse 31400, France
e-mail: renaud.gaudron@centralesupelec.fr

The frequency response of a confined premixed swirled flame is explored experimentally through the use of describing functions that depend on both the forcing frequency and the forcing level. In these experiments, the flame is forced by a loudspeaker connected to the bottom of the burner in the fresh gas region or by a set of loudspeakers connected to the combustion chamber exhaust tube in the burnt gas region. The experimental setup is equipped with a hot-wire (HW) probe and a microphone, both of which located in front of each other below the swirler. The forcing level is varied between $|v'_0|/\overline{v}_0 = 0.10$ *and 0.72 RMS, where* $\overline{v}_0$ *and* v'_0 *are, respectively, the mean and the fluctuating velocity at the HW probe. An additional microphone is placed on a water-cooled waveguide connected to the combustion chamber backplate. A photomultiplier equipped with an OH* filter is used to measure the heat release rate fluctuations. The describing functions between the photomultiplier signal and the different pressure and velocity reference signals are then analyzed in the case of upstream and downstream forcing. The describing function measured for a given reference signal is shown to vary depending on the type of forcing. The impedance of the injector at the HW location is also determined for both upstream and downstream forcing. For all describing functions investigated, it is found that their phase lags do not depend on the forcing level, whereas their gains strongly depend on* $|v'_0|/\overline{v}_0$ *for certain frequency ranges. It is furthermore shown that the flame describing function (FDF) measured with respect to the HW signal can be retrieved from the specific impedance at the HW location and the describing function determined with respect to the signal of the microphone located in front of the HW. This relationship is not valid when the signal from the microphone located at the combustion chamber backplate is considered. It is then shown that a one-dimensional (1D) acoustic model allows to reproduce the describing function computed with respect to the microphone signal inside the injector from the microphone signal located at the combustion chamber backplate in the case of downstream forcing. This relation does not hold for upstream forcing because of the acoustic dissipation across the swirler which is much larger compared to downstream forcing for a given forcing level set at the HW location. This study sheds light on the differences between upstream and downstream acoustic forcing when measuring describing functions. It is also shown that the upstream and downstream forcing techniques are equivalent only if the reference signal used to determine the FDF is the acoustic velocity in the fresh gases just before the flame.*
[DOI: 10.1115/1.4041000]

Introduction

Coupling an acoustic solver with a flame transfer function (FTF), or its nonlinear extension, a flame describing function (FDF), has been shown to be a powerful framework to predict the thermoacoustic stability of practical combustors at a limited computational cost [1–6]. In these low-order models, the flame frequency response to acoustic waves is described by the complex function called FTF and defined as [7]

$$F(\omega) = \frac{\dot{Q}'/\overline{\dot{Q}}}{v'/\overline{v}} \tag{1}$$

where $\dot{Q}$ denotes the heat release rate produced by the flame and v the velocity at some location inside the injector. Throughout this work, the overline stands for the mean conditions and the prime corresponds to the Fourier component of the signal at the forcing angular frequency ω.

The FTF can be generalized to take into account the effect of the forcing level $|v'|/\overline{v}$ [8,9]. In this case, the operator defined in Eq. (1) becomes nonlinear and is called a FDF. This function can then be used to analyze the dynamics of each mode of the combustor and determine the level reached by the acoustic oscillations within the system.

It has been demonstrated that this framework is able to reproduce the nonlinear dynamics of lab-scale combustors equipped with swirling injectors [10,11], and more recently, the nonlinear dynamics of annular systems with multiple flames [6]. One difficulty is to have a good knowledge of the FDF covering the frequency range of interest at low and high perturbation amplitudes [6]. This requires high efficiency actuation systems and acoustic forcing can be generated from the upstream [12,13] or downstream [14] sides of the combustion region.

Another difficulty is to properly define the reference signal used to compute the FDF [15]. This reference signal is sometimes defined as the velocity signal at some location inside the injector [9,16] and sometimes as the velocity signal at the flame location [17–20]. Other authors use the pressure signal inside the combustion chamber as a reference to characterize the nonlinear flame

response [21–23]. However, no systematic comparison between the describing functions defined with these various reference signals has been performed so far.

The aim of this work is to measure and establish a link between various describing functions based on three different reference signals (see Fig. 1):

- The acoustic velocity before the swirler, measured with the hot wire probe labeled HW;
- the acoustic pressure before the swirler, measured with the microphone labeled MHW located at the same axial position as the hot-wire probe;
- the acoustic pressure at the backplate of the combustion chamber, measured with the microphone labeled MC.

A reconstruction of the describing function with a reference signal corresponding to the acoustic velocity inside the injector just before the combustion chamber is also attempted.

The experimental setup is first described, followed by a brief derivation of the analytical links between different describing functions. All three measured describing functions are then compared for upstream and downstream forcing. The analytical links between different describing functions are then tested. A discussion is conducted to interpret the common features and differences observed between the describing functions determined by acoustically forcing the system from the upstream and downstream sides. Finally, an interpretation of the validity of various reconstructions is proposed.

Experimental Setup

The experimental setup in Fig. 1 is used to determine different describing functions. A methane and air mixture is injected in a tranquilization box by two opposed apertures at the bottom of the burner. When upstream forcing is applied, a loudspeaker (Monacor SP-6/108PRO - 100 W RMS) fixed below the tranquilization box is used to generate harmonic acoustic waves. When downstream forcing is applied, this bottom loudspeaker is idle. The flow is then pushed through an antiflashback grid and a honeycomb structure that reduces the turbulence intensity in the plenum. A converging nozzle (contraction ratio: 8.73) generates a fully laminar flow with a top-hat velocity profile.

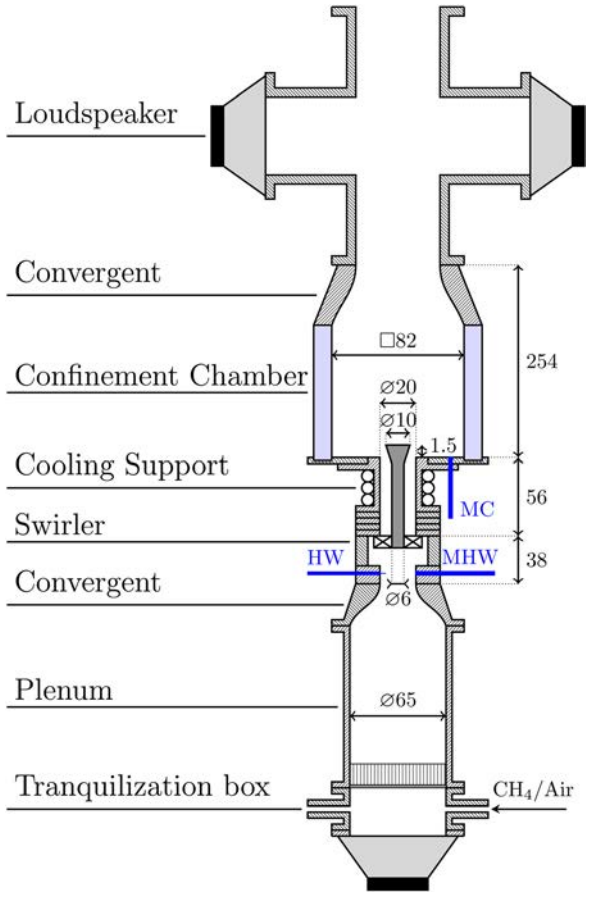

Fig. 1 Experimental setup used to determine various describing functions

A hot-wire probe (Dantec Dynamics Mini-CTA 54T30 with a 55P16 probe) called HW in Fig. 1 is used to determine the mean $\overline{v}_0$ and fluctuating v'_0 velocity signals at the nozzle outlet in the top-hat region of the velocity profile. A microphone (Bruel & Kjaer 4938) called MHW in Fig. 1 and linked to a conditioning amplifier (Bruel & Kjaer 2690) measures the fluctuating pressure signal p'_0 at the same axial position as the hot-wire probe. A swirler with six holes of radius $R = 3$ mm (contraction ratio: 7.41) creates a rotating flow characterized by a swirl number $S = 0.8$. The swirl number was measured by Laser Doppler Velocimetry 2 mm away from the conical bluff body used to stabilize the flame. A cooling support is included to prescribe the combustion chamber backplate temperature. A second microphone (Bruel & Kjaer 4938) called MC in Fig. 1 and mounted on a water-cooled waveguide is used to measure the pressure fluctuations at the combustion chamber backplate. The small acoustical distortions induced by the waveguide are corrected through the use of its transfer function that was determined in a separate set of experiments. Optical access into the combustion chamber is granted by four quartz windows that are transparent for both the visible and the near ultraviolet wavelengths. A second convergent (contraction ratio: 2.03) is added at the top of the combustion chamber through which the burnt gases are exhausted. An additional element is placed above to hold two loudspeakers (Monacor SP-6/108PRO - 100 W RMS) at the top of the exhaust nozzle. This element is used to generate harmonic acoustic waves when downstream forcing is applied or is left idle when upstream forcing is applied.

In addition to the acoustic measurements, a photomultiplier (Hamamatsu H5784-04) equipped with an interferometric filter (Asahi Spectra ZBPA310) centered on $\lambda = 310$ nm and with a 10 nm bandwidth records the OH* chemiluminescence signal, which is assumed to be linearly related to the heat release rate [24]. Different describing functions are deduced from the cross power spectral density between the photomultiplier signal and an arbitrary signal oscillating at the forcing frequency (such as the voltage applied to the loudspeaker) divided by the cross power spectral density between the reference signal and the same arbitrary signal. The reference signals include the HW probe, the microphone located inside the injector (MHW), and the microphone located at the combustion chamber backplate (MC). All time series recorded contain at least 40 oscillation cycles. An ICCD camera (Princeton Instruments PI-MAX 4) equipped with the same band-pass filter (Asahi Spectra ZBPA310) is also used to record the flame chemiluminescence distribution averaged over 100 frames, as presented in Fig. 2. It was checked that the camera collects all the light originating from the flame.

The configuration investigated in this study is a perfectly premixed methane/air flame with an equivalence ratio $\phi = 0.82$ and a thermal power of 5.5 kW. The associated bulk velocity at the hot-wire location, in a tube of diameter $D = 22$ mm, is $U_b = 5.4$ m/s. The highest velocity $v_{\max} = 12$ m/s is reached by the flow inside the six swirler injection holes. It corresponds to a Mach number $M = 0.035$. The mean pressure drop in the test-rig is determined with a differential manometer between the plenum and the ambient pressure and is lower than 400 Pa, corresponding to $\Delta p/\overline{p} = 0.4\%$.

All pressure signals presented in this work are divided by the characteristic impedance $\overline{\rho}\,\overline{c}$, where $\overline{\rho}$ is the mean gas density and $\overline{c}$ the speed of sound at the microphone location. By doing so, the same dimension, a velocity in m/s, is prescribed for the hot-wire

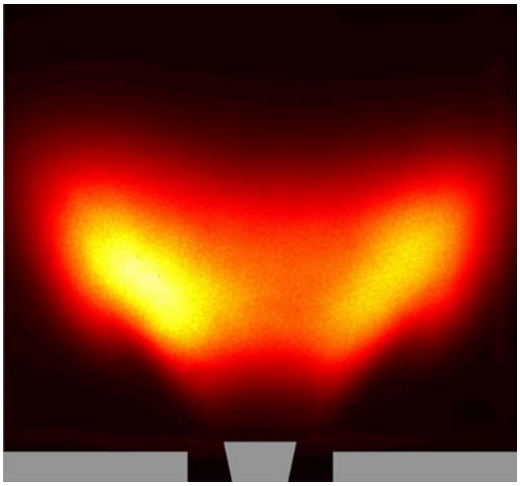

Fig. 2 Mean OH* chemiluminescence distribution for steady flow injection conditions. $\phi = 0.82$, $U_b = 5.4$ m/s.

and normalized microphone signals thus simplifying the comparison between the various describing functions that are introduced in the following section. The original expressions can be easily retrieved by doing the reverse operation.

Links Between the Describing Functions

Three describing functions are measured in this work. The first describing function F_{HW} is defined with respect to the HW probe signal

$$F_{\mathrm{HW}}\left(\omega, |v_0'|/\overline{v}_0\right) = \frac{\dot{Q}'/\overline{\dot{Q}}}{v_0'/\overline{v}_0} \tag{2}$$

where the fluctuating $\dot{Q}'$ and the average $\overline{\dot{Q}}$ heat release rate are assessed at the same forcing frequency as the fluctuating v_0' and average $\overline{v}_0$ velocity at the hot-wire probe. The flame nonlinearities are taken into account by including the forcing level $|v_0'|/\overline{v}_0$ as one of the variables of the describing function.

The second describing function F_{MHW} is defined with respect to the microphone located inside the injector (MHW) in front of the hot-wire

$$F_{\mathrm{MHW}}\left(\omega, |v_0'|/\overline{v}_0\right) = \frac{\dot{Q}'/\overline{\dot{Q}}}{p_0'/\overline{p}_0} \tag{3}$$

where p_0' is the fluctuating pressure signal measured by MHW (See Fig. 1) and p_0 is taken equal to the atmospheric pressure divided by the characteristic impedance $\overline{\rho}_0\overline{c}_0$ at the hot-wire location.

The third describing function F_{MC} is defined with respect to the microphone located at the bottom of the combustion chamber (MC)

$$F_{\mathrm{MC}}\left(\omega, |v_0'|/\overline{v}_0\right) = \frac{\dot{Q}'/\overline{\dot{Q}}}{p_8'/\overline{p}_8} \tag{4}$$

where p_8' is the fluctuating pressure signal measured by MC and $\overline{p}_8$ is a constant that has the same dimension as p_8'. The quantity $\overline{p}_8$ is taken equal to the atmospheric pressure divided by the characteristic impedance $\overline{\rho}_8\overline{c}_8$ in the burnt gases, at the bottom of the combustion chamber.

A fourth describing function F_{HWC} is defined with respect to the acoustic velocity v_7' at the injector outlet, just before the combustion chamber

$$F_{\mathrm{HWC}}\left(\omega, |v_0'|/\overline{v}_0\right) = \frac{\dot{Q}'/\overline{\dot{Q}}}{v_7'/\overline{v}_7} \tag{5}$$

where $\overline{v}_7$ and v_7' are, respectively, the mean and fluctuating velocity at the injector outlet. This describing function, generally designated as the FDF [9,20], is not measured in the present work and is deduced from the previous describing functions using the models described thereafter.

It is worth recalling that the forcing level is always prescribed at the same axial location, the hot-wire location, which explains why the variable $|v_0'|/\overline{v}_0$ is the same for all describing functions in Eqs. (2)–(5).

The link between F_{HW} and F_{MHW} is straight-forward since the hot-wire HW and the microphone MHW are located in front of each other at the same axial position. By introducing the dimensionless specific acoustic impedance $z = Z/(\overline{\rho}_0\overline{c}_0)$ at the hot-wire location, one obtains

$$F_{\mathrm{HW}}\left(\omega, |v_0'|/\overline{v}_0\right) = z(\omega)\frac{\overline{v}_0}{\overline{p}_0}F_{\mathrm{MHW}}\left(\omega, |v_0'|/\overline{v}_0\right) \tag{6}$$

It has been checked (not shown here) that z remains independent of the forcing level, i.e., the burner acoustic response upstream the hot-wire remains in the linear regime. This expression is later used to check for the consistency of the measurements.

In order to relate F_{MC} to F_{MHW} and to F_{HW}, a link between the acoustic pressure p_8' at the bottom of the combustion chamber and the acoustic variables p_0' and v_0' at the hot-wire location has to be established. The acoustic model representing the injector dynamics is depicted in Fig. 3. It comprises eight elements for which the downstream acoustic variables have to be related to the upstream acoustic variables. The hot-wire probe HW and the microphone MHW are located in section (0). The swirler is comprised between sections (3) and (6) and the combustion chamber starts in section (8), where MC is placed. In this work, the index k refers to variables assessed in section (k). The change in temperature from $T_u = 293$ K in the fresh gas region to $T_b = 1200$ K in the burnt gas region is also accounted for.

Assuming one-dimensional (1D) linear acoustic wave propagation in the burner [25,26], one is left with

$$p_8' = (T_b/T_u)^{1/2}(p_0' - ikL_a v_0') \tag{7}$$

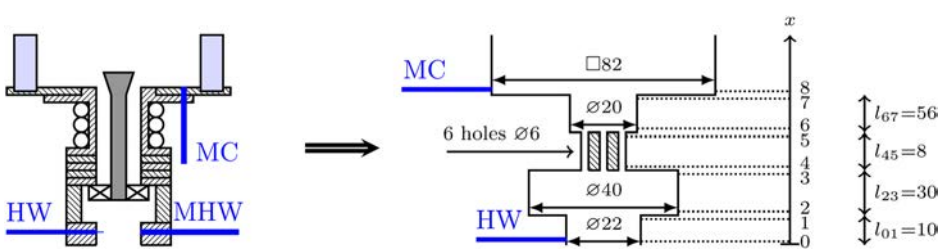

Fig. 3 Zoomed view on the injector and acoustic model representing the injector dynamics. All dimensions are in mm.

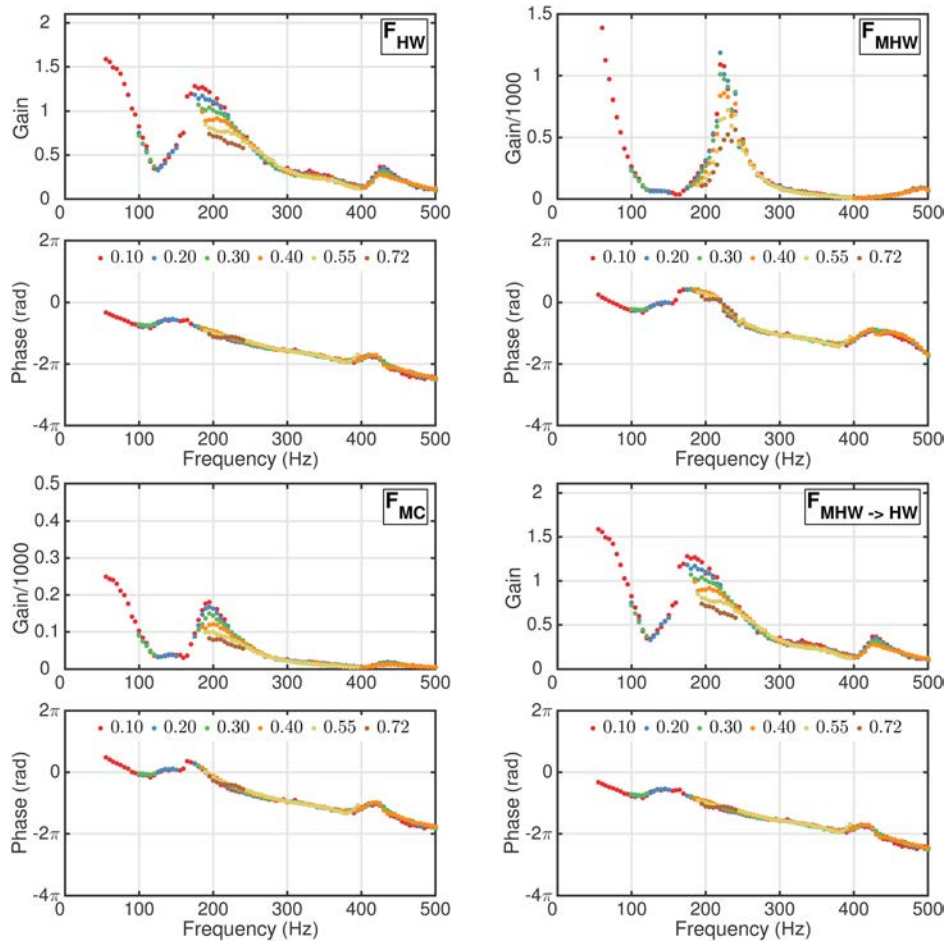

Fig. 4 Describing functions obtained with downstream forcing for six different forcing levels $|v'_0|/\overline{v}_0$ measured at the HW location. F_{HW}: $(\dot{Q}'/\overline{\dot{Q}})/(v'_0/\overline{v}_0)$; F_{MHW}: $(\dot{Q}'/\overline{\dot{Q}})/(p'_0/\overline{p}_0)$; F_{MC}: $(\dot{Q}'/\overline{\dot{Q}})/(p'_8/\overline{p}_8)$; and $F_{MHW\to HW} = z\overline{v}_0 F_{MHW}/\overline{p}_0$.

where p'_0 and v'_0 are, respectively, the acoustic pressure and velocity measured by MHW and HW in section (0) of the network model in Fig. 3 and p'_8 is the acoustic pressure in section (8). In this expression, the complex waves are determined with the $\exp(i\omega t)$ harmonic convention and the pressure signals are divided by their respective characteristic impedances thus explaining the presence of the fresh and burnt gas temperatures in Eq. (7). The length L_a takes into account wave propagation between sections (0) and (8)

$$L_a = l_{01} + l_{23}\left(\frac{S_1}{S_2}\right) + l_{45}\left(\frac{S_1}{S_4}\right) + l_{67}\left(\frac{S_1}{S_6}\right) \tag{8}$$

where S_j denotes the cross section area at the axial position j and l_{ij} the length of the element between the axial positions i and j in Fig. 3. Using Eqs. (7) and (8), the describing functions F_{MC} and F_{MHW} are connected by

$$F_{MC}\left(\omega, |v'_0|/\overline{v}_0\right) = F_{MHW}\left(\omega, |v'_0|/\overline{v}_0\right)\frac{1}{(1 - ikL_a/z)} \tag{9}$$

Equations (7) and (8) and subsequently Eq. (9) are only valid at low frequencies [27], when the Helmholtz number $He = kL_a$ remains small. In this work, the maximum frequency investigated is $f_{max} = 500$ Hz corresponding to a maximum Helmholtz number $He = 0.98$. Hence, the previous condition is respected and Eqs. (7)–(9) are applicable to the investigated configuration. Furthermore, this maximum Helmholtz number is small enough to justify the use of the hot-wire HW and microphone MHW as reference signals.

It is worth mentioning that acoustic diffraction [28] at different jumps in cross section area, acoustic dissipation due to viscous dissipation and acoustic dissipation inside the swirler holes due to the interaction of acoustic waves with vortical structures [29] are not taken into account in this reconstruction. Moreover, since the mean pressure drop across the setup remains small ($\Delta p/\overline{p} = 0.4\%$) and the Mach number is much smaller than unity ($M = 0.035$), the mean pressure drop effects are neglected in this work [25].

The same procedure is applied to link the acoustic velocity v'_7 at the injector outlet to the acoustic velocity v'_0 and the acoustic pressure p'_0 at the hot-wire location

$$v'_7 = (S_1/S_6)(v'_0 - ikL_b p'_0) \tag{10}$$

with L_b defined as

$$L_b = l_{01} + l_{23}\left(\frac{S_2}{S_1}\right) + l_{45}\left(\frac{S_4}{S_1}\right) + l_{67}\left(\frac{S_6}{S_1}\right) \tag{11}$$

Using Eqs. (10) and (11), the describing functions F_{HW} and F_{HWC} are connected by

$$F_{HWC}\left(\omega, |v'_0|/\overline{v}_0\right) = F_{HW}\left(\omega, |v'_0|/\overline{v}_0\right)\frac{1}{(1 - ikL_b z)} \tag{12}$$

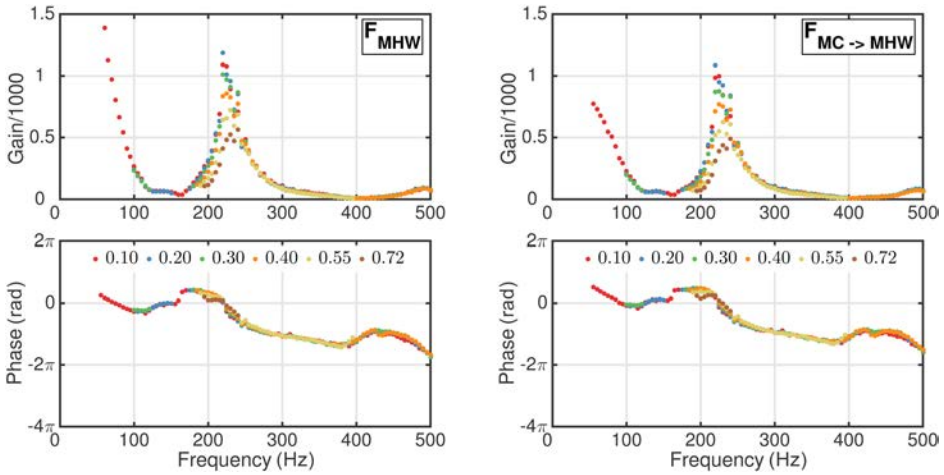

Fig. 5 Describing function determined with microphone MHW and its reconstruction from microphone MC and Eq. (9). Results are shown for six forcing levels $|v'_0|/\bar{v}_0$ and for downstream forcing.

The validity of Eqs. (6) and (9) is now assessed by comparing the measured describing functions with their associated reconstructions from these equations.

Results

Downstream Forcing. A first set of experiments is conducted with downstream forcing. The three describing functions, F_{HW}, F_{MHW} and F_{MC}, defined in the previous section are extracted from measurements. Results are presented in Fig. 4 with $F_{\mathrm{HW}}(\omega, |v'_0|/\bar{v}_0)$ at the top left, $F_{\mathrm{MHW}}(\omega, |v'_0|/\bar{v}_0)$ at the top right, and $F_{\mathrm{MC}}(\omega, |v'_0|/\bar{v}_0)$ at the bottom left. Finally, the plots at the bottom right represent $F_{\mathrm{MHW}\to\mathrm{HW}}(\omega, |v'_0|/\bar{v}_0)$, a reconstruction of $F_{\mathrm{HW}}(\omega, |v'_0|/\bar{v}_0)$ using data gathered for $F_{\mathrm{MHW}}(\omega, |v'_0|/\bar{v}_0)$ by the means of the specific impedance z as expressed in Eq. (6). For each describing function, the flame frequency response is measured for six different forcing levels set at the hot-wire location $|v'_0|/\bar{v}_0 = 0.10$, 0.20, 0.30, 0.40, 0.55, and 0.72 RMS and the top and bottom plots represent the describing function gain and phase lag, respectively.

An important feature is that for all three describing functions F_{HW}, F_{MHW}, and F_{MC}, the gain plots in Fig. 4 depend on the forcing level $|v'_0|/\bar{v}_0$ for frequencies comprised between 180 Hz and 250 Hz. At lower and higher frequencies, the gain remains independent of the input level $|v'_0|/\bar{v}_0$. Furthermore, the phase lag plots of these describing functions remain independent of the forcing level over the full frequency range. This last feature is often observed for fully premixed swirling flames [30].

Results for $F_{\mathrm{HW}}(\omega, |v'_0|/\bar{v}_0)$ are now compared with $F_{\mathrm{MHW}\to\mathrm{HW}}(\omega, |v'_0|/\bar{v}_0)$, the reconstruction obtained from $F_{\mathrm{MHW}}(\omega, |v'_0|/\bar{v}_0)$. Both the gain and phase lag plots of F_{HW} and $F_{\mathrm{MHW}\to\mathrm{HW}}$ are identical in Fig. 4 for all forcing levels and all frequencies. This proves that the measurements of the specific impedance z and the describing functions F_{HW} and F_{MHW} are reliable and reproducible. It also proves that the describing functions $F_{\mathrm{HW}}(\omega, |v'_0|/\bar{v}_0)$ and $F_{\mathrm{MHW}}(\omega, |v'_0|/\bar{v}_0)$ measured with the hot-wire probe and the microphone installed in vis-a-vis are fully equivalent as long as the specific impedance z at the hot-wire location is known.

The describing functions $F_{\mathrm{MHW}}(\omega, |v'_0|/\bar{v}_0)$ and $F_{\mathrm{MC}}(\omega, |v'_0|/\bar{v}_0)$, respectively determined with the microphone in the injector (MHW) and in the combustion chamber (MC), are now compared. The gain plots of F_{MHW} and F_{MC} feature roughly the same type of evolution in Fig. 4 except that gain values for $F_{\mathrm{MHW}}(\omega, |v'_0|/\bar{v}_0)$ with the microphone set before the swirler are about ten times larger than the ones found for the describing function $F_{\mathrm{MC}}(\omega, |v'_0|/\bar{v}_0)$ determined with the microphone located in the combustion chamber. Moreover, there is a slight phase shift between the phase lags measured for $F_{\mathrm{MHW}}(\omega, |v'_0|/\bar{v}_0)$ and $F_{\mathrm{MC}}(\omega, |v'_0|/\bar{v}_0)$ due to acoustic wave propagation between the hot-wire location and the bottom of the combustion chamber.

The next step is to compare the describing function $F_{\mathrm{MHW}}(\omega, |v'_0|/\bar{v}_0)$ and the associated reconstruction $F_{\mathrm{MC}\to\mathrm{MHW}}(\omega, |v'_0|/\bar{v}_0)$ obtained from $F_{\mathrm{MC}}(\omega, |v'_0|/\bar{v}_0)$ using Eq. (9). Results are shown in Fig. 5. The acoustic model given by Eq. (9) yields an excellent reconstruction for the gain and phase lag over the entire frequency range and for all forcing levels. It is reminded that these results are obtained by forcing the system from the downstream side with the oscillation level measured by the hot-wire probe below the swirler.

Upstream Forcing. A second set of experiments is conducted with acoustic forcing from the upstream side. As for the downstream forcing case, the signals corresponding to the hot-wire probe, the microphones, and the photomultiplier are measured for the same forcing levels controlled by the hot-wire probe. The three resulting describing functions F_{HW}, F_{MHW}, and F_{MC} are determined from these data and plotted in Fig. 6. Again, the plots at the bottom right represent $F_{\mathrm{MHW}\to\mathrm{HW}}(\omega, |v'_0|/\bar{v}_0)$, the reconstruction of $F_{\mathrm{HW}}(\omega, |v'_0|/\bar{v}_0)$ using the data from $F_{\mathrm{MHW}}(\omega, |v'_0|/\bar{v}_0)$ and Eq. (6).

A common feature between upstream and downstream forcing experiments is that the phase lag plots of all measured describing functions in Figs. 4 and 6 are independent of the forcing level at all frequencies. This means that the describing function phase lag can be safely determined without considering the effects of the forcing level. Moreover, the phase lag plots of $F_{\mathrm{HW}}(\omega, |v'_0|/\bar{v}_0)$ coincide for upstream and downstream forcing experiments implying that the way acoustic forcing is introduced in the system has no impact on the phase lag plot of the describing function computed with respect to the hot-wire signal.

However, there are also differences between results obtained with downstream and upstream forcing. The gain plots of $F_{\mathrm{HW}}(\omega, |v'_0|/\bar{v}_0)$ and $F_{\mathrm{MHW}}(\omega, |v'_0|/\bar{v}_0)$ in Fig. 6 now depend on the forcing level $|v'_0|/\bar{v}_0$ for frequencies comprised between 20 Hz and 100 Hz and between 180 Hz and 250 Hz, while with downstream forcing, the gain plots of $F_{\mathrm{HW}}(\omega, |v'_0|/\bar{v}_0)$ and $F_{\mathrm{MHW}}(\omega, |v'_0|/\bar{v}_0)$ in Fig. 4 depend on the forcing level only between 180 Hz and 250 Hz. It should be noted that this difference comes from the limited low-frequency range explored with downstream forcing due to technical limitations. Acoustic forcing from the downstream side requires a higher power than experiments

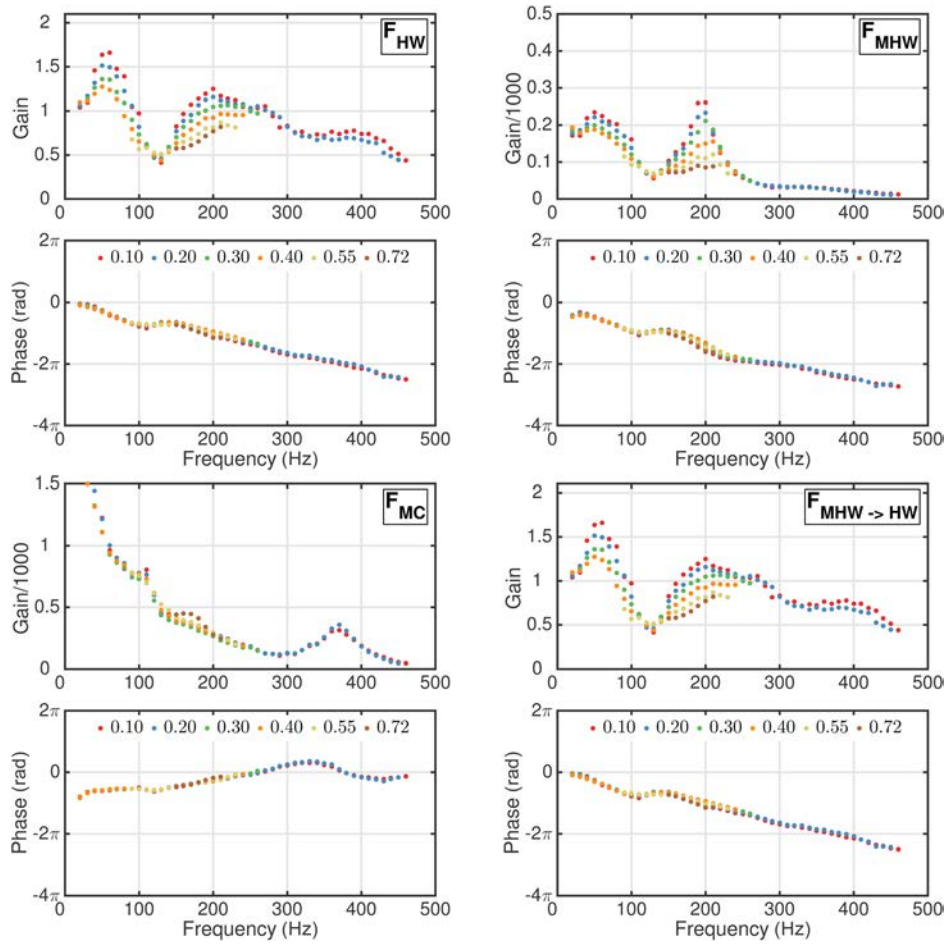

Fig. 6 Describing functions obtained with upstream forcing for six different forcing levels $|v_0'|/\overline{v}_0$ measured at the HW location. F_{HW}: $(\dot{Q}'/\overline{\dot{Q}})/(v_0'/\overline{v}_0)$; F_{MHW}: $(\dot{Q}'/\overline{\dot{Q}})/(p_0'/\overline{p}_0)$; F_{MC}: $(\dot{Q}'/\overline{\dot{Q}})/(p_8'/\overline{p}_8)$; and $F_{MHW\rightarrow HW} = z\overline{v}_0 F_{MHW}/\overline{p}_0$.

conducted with upstream excitation to get the same oscillation level at the hot-wire location, especially at low frequencies.

On the other hand, the gain plot of the describing function $F_{MC}(\omega, v_0'|/\overline{v}_0)$ in Fig. 6 obtained with upstream forcing now remains almost independent of the forcing level for all forcing frequencies. This is again in contrast with the results presented for $F_{MC}(\omega, |v_0'|/\overline{v}_0)$ in Fig. 4 determined with downstream forcing experiments. Moreover, the evolution of the gain of F_{MC} with the forcing frequency in the bottom left plots in Figs. 4 and 6 significantly differs depending on the type of forcing. This is due to the difference in acoustic pressure levels inside the combustion chamber between experiments conducted with upstream and downstream acoustic forcing. For a given oscillation level measured by the hot-wire inside the injector, downstream excitation results in a much larger pressure oscillation level at the bottom of the combustion chamber than upstream forcing. Furthermore, for upstream forcing, the acoustic pressure at the bottom of the combustion chamber rapidly drops toward zero as the forcing frequency decreases thus explaining why the gain of $F_{MC}(\omega, |v_0'|/\overline{v}_0)$ rapidly increases at low frequencies.

It is now worth exploring if different describing functions F_{HW}, F_{MHW}, and F_{MC} can be reconstructed from one another in the case of upstream forcing. The describing function $F_{HW}(\omega, |v_0'|/\overline{v}_0)$ and the associated reconstruction $F_{MHW\rightarrow HW}(\omega, |v_0'|/v_0)$ deduced from $F_{MHW}(\omega, |v_0'|/\overline{v}_0)$ and Eq. (6) are again found to be identical for all frequencies and forcing levels in Fig. 6. This consistency check once again validates the data gathered for the specific impedance z at the hot-wire location and the describing functions F_{HW} and F_{MHW}. It also shows that z depends on the type of forcing. Furthermore, determining $F_{HW}(\omega, |v_0'|/\overline{v}_0)$ or $F_{MHW}(\omega, |v_0'|/\overline{v}_0)$ is once again equivalent as long as the specific impedance z at the hot-wire location is known with precision.

The describing functions F_{MHW} determined with the microphone in front of the hot-wire and F_{MC} determined with the microphone at the bottom of the combustion chamber are now further examined. The shapes taken by $F_{MHW}(\omega, |v_0'|/\overline{v}_0)$ and $F_{MC}(\omega, |v_0'|/\overline{v}_0)$ differ in Fig. 6. The main differences are that $F_{MC}(\omega, |v_0'|/\overline{v}_0)$ does not depend on the forcing level $|v_0'|/\overline{v}_0$ and that the peaks observed in all other describing functions are absent in the gain plot of $F_{MC}(\omega, |v_0'|/\overline{v}_0)$. In addition, the gain at zero frequency does not reach a fixed level but rapidly increases, as explained previously. Finally, the phase lag plot increases as the forcing frequency increases. Figure 7 shows that the reconstruction $F_{MC\rightarrow MHW}(\omega, |v_0'|/\overline{v}_0)$ of $F_{MHW}(\omega, |v_0'|/\overline{v}_0)$ from the data gathered for $F_{MC}(\omega, |v_0'|/\overline{v}_0)$ and the acoustic model given by Eq. (9) does not yield the correct result when the system is acoustically forced from the upstream side.

Discussion

It is known that reliable predictions of thermo-acoustic instability oscillation frequencies and limit cycle levels can be achieved by combining the flame describing function F_{HW} determined with a velocity reference signal with different types of acoustic solvers [9,10]. In many works, the relation F_{HW} between heat release rate

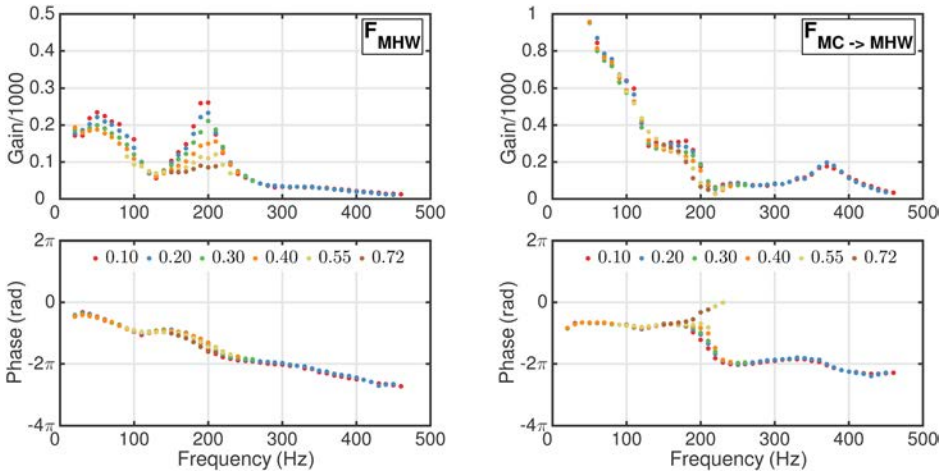

Fig. 7 Describing function determined with microphone MHW and its reconstruction from microphone MC and Eq. (9). Results are shown for six forcing levels $|v'_0|/\overline{v}_0$ and for upstream forcing.

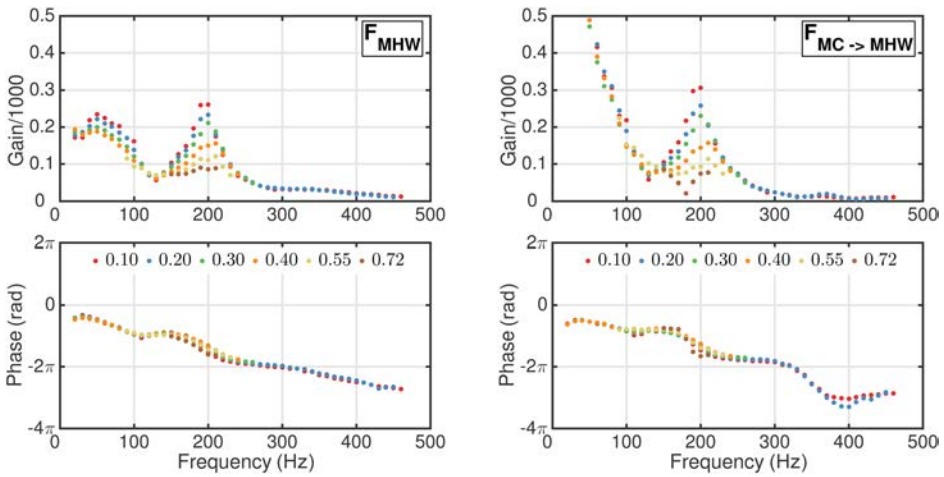

Fig. 8 Describing function determined with microphone MHW and its reconstruction from microphone MC and the new model accounting for acoustic dissipation at the swirler holes according to Eq. (13). Results are shown for six forcing levels $|v'_0|/\overline{v}_0$ and for upstream forcing.

and velocity disturbances remains unknown and is difficult to determine in practical combustors. The relation F_{HW} is thus often replaced by a relation between heat release rate and pressure fluctuations measured at some location in the combustion chamber and designated by F_{MC} in this work. It appears that the downstream forcing technique is the only one allowing to reconstruct the FDF F_{HW} from the describing function F_{MC} by means of a linear acoustic model. This linear model accounts for acoustic propagation and the effects of sudden area changes but all dissipation mechanisms are neglected. However, it is known that an important source of acoustic damping within the flow comes from the coupling between vortical structures generated in shear layers and acoustic waves [31–33].

The model of Howe [32] for an aperture traversed by a high-Reynolds bias flow is used here in order to model the acoustic pressure drop through the swirler between sections (3) and (6) in Fig. 3, where the mean and fluctuating velocities are the largest. Using the notations introduced previously, the acoustic pressure drop across the swirler is given by

$$\overline{\rho}_3 S_3 u'_3 = \overline{\rho}_6 S_6 u'_6 = -K_r(p'_6 - p'_3) \tag{13}$$

where $u'_3 S_3$ is the acoustic volume flow rate fluctuation in section (3) and K_r is the Rayleigh conductivity of the aperture given in Ref. [32].

A refined model based on Eqs. (7) and (10) but accounting for the acoustic losses at the swirler through Eq. (13) is now used to compare $F_{\mathrm{MHW}}(\omega, |v'_0|/\overline{v}_0)$ and the associated reconstruction $F_{\mathrm{MC}\to\mathrm{MHW}}(\omega, |v'_0|/\overline{v}_0)$ of $F_{\mathrm{MHW}}(\omega, |v'_0|/\overline{v}_0)$ from the data gathered for $F_{\mathrm{MC}}(\omega, |v'_0|/\overline{v}_0)$ based on this new model. The results are plotted in Fig. 8.

It is clear from Fig. 8 that the new reconstruction including the effects of the acoustic pressure drop across the swirler yields much better results than the original model without acoustic dissipation. The overall shape of both the gain and phase lag plots of F_{MHW} are retrieved accurately, except in the low-frequency region, where the number of forcing cycles used to determine the describing function F_{MC} is limited, and hence, the predictions worsen. The correct evolution of F_{MHW} with the forcing level $|v'_0|/\overline{v}_0$ is also retrieved with this new model. As a conclusion, it is necessary to take into account the acoustic pressure drop across the swirler when linking various describing functions in the case of upstream forcing.

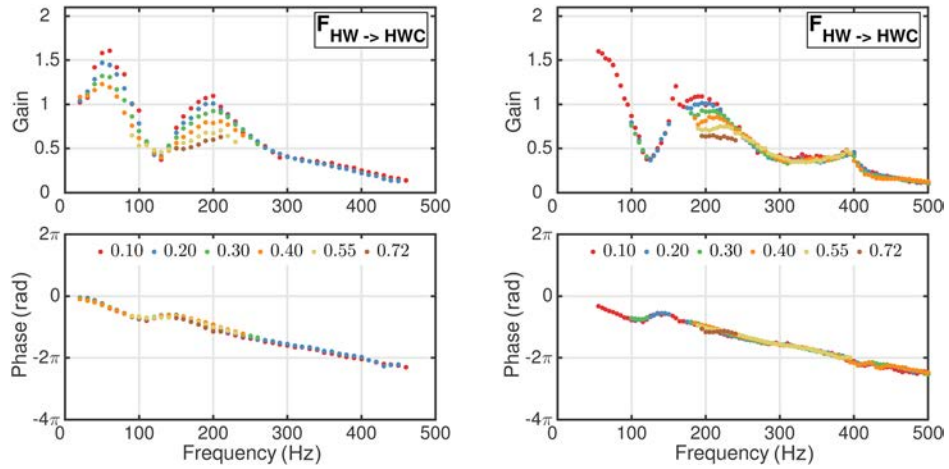

Fig. 9 Reconstructed FDFs with respect to the acoustic velocity at the injector outlet (section (7) in Fig. 3) for six different forcing levels $|v'_0|/\bar{v}_0$ measured by the HW probe. Left: upstream forcing; right: downstream forcing.

The same comparison is made for downstream forcing (not shown here). In that case, the reconstruction of F_{MHW} from F_{MC} with the improved model turns out to be almost equivalent to the previous simple linear model corresponding to Eq. (9). It is not necessary to take into account the acoustic pressure drop across the swirler when linking various describing functions in the case of downstream forcing.

One important conclusion of this work is that the dynamical state of the system is not symmetric for upstream and downstream forcing. This is attributed to the fact that the upstream and downstream acoustic boundary conditions differ depending on the type of forcing. As a consequence, the structure and level of the acoustic pressure field differs for upstream and downstream forcing, as depicted in Figs. 4 and 6. This in turn has an impact on the acoustic pressure drop across the swirler. For upstream forcing, this acoustic pressure drop is large, whereas it is negligible for downstream forcing.

The experiments conducted in this work also reveal that the FDF $F_{\mathrm{HW}}(\omega, |v'_0|/\bar{v}_0)$ based on the acoustic velocity before the swirler can be determined with upstream or downstream acoustic forcing experiments. Slight differences, however, are observed between results for F_{HW} in Fig. 4 and those shown in Fig. 6. Both methods yield the same results for the phase lag at all frequencies and velocity modulation amplitudes. The gain plots are also the same for forcing frequencies lower than 220 Hz. Differences appear in the high frequency region. The FDF gain plot rapidly drops below unity for $f > 220$ Hz and is strongly attenuated with gains lower than 0.5 when $f > 270$ Hz in the case of downstream forcing. When the flame is modulated from the upstream side, the FDF gain remains relatively large and above 0.5 in Fig. 6 up to $f = 440$ Hz at the low forcing levels $|v'_0|/\bar{v}_0 = 0.1$ and 0.2 RMS.

These differences can be reduced by reconstructing the describing function $F_{\mathrm{HWC}}(\omega, |v'_0|/\bar{v}_0)$ defined with respect to the acoustic velocity at the injector outlet in section (7) (see Fig. 3) from $F_{\mathrm{HW}}(\omega, |v'_0|/\bar{v}_0)$ and the acoustic model corresponding to Eq. (12). In that case, the match between the plots for $F_{\mathrm{HWC}}(\omega, |v'_0|/\bar{v}_0)$ in Fig. 9 corresponding to upstream and downstream forcing is almost perfect for all frequencies and all forcing levels. This comparison confirms that the flame describing function depends on flowrate disturbances only (and not on the acoustic pressure) when the velocity reference is close enough to the flame. This extends a previous result obtained in the linear regime for laminar flames [15] to swirled flames forced at any perturbation amplitude.

Finally, the describing functions $F_{\mathrm{MHW}}(\omega, |v'_0|/\bar{v}_0)$ determined with the microphone in front of the hot-wire probe largely differ in terms of gain and phase lag with downstream and upstream forcing. For instance, the maximum gain achieved with downstream forcing is around 1200 in Fig. 4 compared to 300 with upstream forcing in Fig. 6. This is due to the fact that the specific impedance z at the hot-wire location depends on the type of forcing since the acoustic boundary condition at the hot-wire location varies in these two cases. This impedance represents the acoustic response seen by MHW and HW from all the components below these sensors when the system is perturbed from the downstream or upstream sides.

Conclusion

The response of a confined premixed swirling flame submitted to acoustic forcing from the upstream and downstream sides of a combustor has been determined for a large set of forcing frequencies and forcing levels. Three types of describing functions relating heat release rate fluctuations to different reference signals have been defined. The first reference signal is the acoustic velocity inside the injector measured by a hot-wire probe below the swirler. The second reference signal is the acoustic pressure measured by a microphone at the same axial location as the hot-wire probe. The third reference signal corresponds to the acoustic pressure inside the combustion chamber determined with a microphone mounted on a water-cooled waveguide. The forcing level is in all cases controlled by the hot-wire probe.

For downstream acoustic forcing experiments, the gain plots of these different describing functions change with the forcing level over a certain frequency range, whereas the phase lag plots remain independent of the forcing level. It has been found that all three describing functions could be reconstructed from one another using a linear acoustic model linking the acoustic pressure at the combustion chamber backplate to the acoustic pressure inside the injector, at the hot-wire location.

It has also been verified that for both downstream and upstream acoustic forcing experiments, the specific impedance z at the hot-wire location could be used to reconstruct the describing function based on the hot-wire signal from the describing function based on the facing microphone signal and vice versa.

For upstream acoustic forcing experiments, the same describing functions as for downstream acoustic forcing experiments have been extracted from measurements. In this case, the describing function defined with respect to the acoustic pressure measured at the hot-wire location could not be reconstructed from the describing function defined with respect to the microphone located at the combustion chamber backplate through the use of a 1D linear acoustic model of the injector. This has been attributed to the fact that the upstream and downstream acoustic boundary conditions

are modified depending on the type of forcing, which in turn modifies the acoustic fields inside the system. A large acoustic pressure drop due to acoustic losses is generated across the swirler in the case of upstream forcing. If this acoustic pressure drop is taken into account in the model, the describing function determined with the acoustic pressure measured inside the injector can be reconstructed from the describing function determined with the acoustic pressure measured inside the combustion chamber. On the other hand, when downstream forcing is applied, the acoustic pressure drop across the swirler is negligible and it is not necessary to consider it to link these two describing functions accurately.

Another important finding is that the gain and phase lag of the FDF linking heat release rate and velocity fluctuations measured by the hot-wire inside the injector are identical for upstream and downstream acoustic forcing as long as the forcing frequency is lower than $f < 220$ Hz. At higher frequencies, both FDF phase lags still match, but the FDF gain drops more rapidly with the forcing frequency for downstream acoustic forcing than for upstream acoustic forcing. The reconstructed describing functions with respect to the acoustic velocity at the injector outlet are found to be almost identical for upstream and downstream forcing experiments at all frequencies and all forcing levels. It is concluded that the describing functions between heat release rate and acoustic fluctuations determined with upstream and downstream forcing are equivalent as long as the reference signal is the acoustic velocity in the fresh gases as close as possible to the flame. For all other reference signals, including the acoustic velocity in the injector below the swirler or the acoustic pressure anywhere in the system, upstream and downstream acoustic forcing appears as nonequivalent techniques to determine the describing function.

These experiments highlight for the first time that the frequency response of a perturbed reacting flow described in terms of heat release rate versus pressure oscillations inside the combustion chamber depends on the way acoustic forcing is introduced in the system. Differences for the resulting describing functions are due to different acoustic pressure and velocity states inside the combustion chamber that are produced by the excitation for a given level of velocity oscillation measured inside the injector, at the hot-wire location.

Acknowledgment

This work is supported by Agence Nationale de la Recherche, NOISEDYN project (ANR-14-CE35-0025-01). This project has received funding from the European Union as Horizon 2020 research and innovation programme under the Marie Sklodowska-Curie Grant agreement no 643134. The authors are thankful to the technical staff of EM2C laboratory for their help.

References

[1] Keller, J. J., 1995, "Thermoacoustic Oscillations in Combustion Chambers of Gas Turbines," AIAA J., **33**(12), pp. 2280–2287.
[2] Dowling, A. P., and Stow, S. R., 2003, "Acoustic Analysis of Gas Turbine Combustors," J. Propul. Power, **19**(5), pp. 751–764.
[3] Sattelmayer, T., and Polifke, W., 2003, "Assessment of Methods for the Computation of Linear Stability of Combustors," Combust. Sci. Technol., **175**(3), pp. 453–476.
[4] Nicoud, F., Benoit, L., Sensiau, C., and Poinsot, T., 2007, "Acoustic Modes in Combustors With Complex Impedances and Multidimensional Active Flames," AIAA J., **45**(2), pp. 426–441.
[5] Camporeale, S. M., Fortunato, B., and Campa, G., 2011, "A Finite Element Method for Three-Dimensional Analysis of Thermo-Acoustic Combustion Instability," ASME J. Eng. Gas Turbines Power, **133**(1), p. 011506.
[6] Laera, D., Schuller, T., Prieur, K., Durox, D., and Camporeale, S. M., 2017, "Flame Describing Function Analysis of Spinning and Standing Modes in an Annular Combustor and Comparison With Experiments," Combust. Flame, **184**, pp. 136–152.
[7] Candel, S., 2002, "Combustion Dynamics and Control: Progress and Challenges," Proc. Combust. Inst., **29**(1), pp. 1–28.
[8] Dowling, A. P., 1997, "Nonlinear Self-Excited Oscillations of a Ducted Flame," J. Fluid Mech., **346**, pp. 271–290.
[9] Noiray, N., Durox, D., Schuller, T., and Candel, S., 2008, "A Unified Framework for Nonlinear Combustion Instability Analysis Based on the Flame Describing Function," J. Fluid Mech., **615**, p. 139.
[10] Palies, P., Durox, D., Schuller, T., and Candel, S., 2011, "Nonlinear Combustion Instability Analysis Based on the Flame Describing Function Applied to Turbulent Premixed Swirling Flames," Combust. Flame, **158**(10), pp. 1980–1991.
[11] Ćosić, B., Moeck, J. P., and Paschereit, C. O., 2014, "Nonlinear Instability Analysis for Partially Premixed Swirl Flames," Combust. Sci. Technol., **186**(6), pp. 713–736.
[12] Boudy, F., Durox, D., Schuller, T., Jomaas, G., and Candel, S., 2011, "Describing Function Analysis of Limit Cycles in a Multiple Flame Combustor," ASME J. Eng. Gas Turbines Power, **133**(6), p. 061502.
[13] Mirat, C., Durox, D., and Schuller, T., 2015, "Stability Analysis of a Swirl Spray Combustor Based on Flame Describing Function," Proc. Combust. Inst., **35**(3), pp. 3291–3298.
[14] Hochgreb, S., Dennis, D., Ayranci, I., Bainbridge, W., and Cant, S., 2013, "Forced and Self-Excited Instabilities From Lean Premixed, Liquid-Fuelled Aeroengine Injectors at High Pressures and Temperatures," ASME Paper No. GT2013-95311.
[15] Truffin, K., and Poinsot, T., 2005, "Comparison and Extension of Methods for Acoustic Identification of Burners," Combust. Flame, **142**(4), pp. 388–400.
[16] Gatti, M., Gaudron, R., Mirat, C., and Schuller, T., 2017, "Effects of the Injector Design on the Transfer Function of Premixed Swirling Flames,"ASME Paper No. GT2017-638.
[17] Gaudron, R., Gatti, M., Mirat, C., and Schuller, T., 2017, "Analysis of the Transfer Function of Large and Small Premixed Laminar Conical Flames," ASME Paper No. GT2017-64231.
[18] Schuller, T., Durox, D., and Candel, S., 2003, "Self-Induced Combustion Oscillations of Laminar Premixed Flames Stabilized on Annular Burners," Combust. Flame, **135**(4), pp. 525–537.
[19] Birbaud, A. L., Durox, D., Ducruix, S., and Candel, S., 2007, "Dynamics of Free Jets Submitted to Upstream Acoustic Modulations," Phys. Fluids, **19**, p. 013602.
[20] Durox, D., Schuller, T., Noiray, N., and Candel, S., 2009, "Experimental Analysis of Nonlinear Flame Transfer Functions for Different Flame Geometries," Proc. Combust. Inst., **32**(1), pp. 1391–1398.
[21] Schuermans, B., Paschereit, C. O., and Monkewitz, P., "Non-Linear Combustion Instabilities in Annular Gas-Turbine Combustors," AIAA Paper No. AIAA 2006-549.
[22] Noiray, N., and Schuermans, B., 2013, "On the Dynamic Nature of Azimuthal Thermoacoustic Modes in Annular Gas Turbine Combustion Chambers," Proc. R. Soc. A, **469**, p. 20120535.
[23] Ghirardo, G., Juniper, M. P., and Moeck, J. P., 2015, "Stability Criteria for Standing and Spinning Waves in Annular Combustors," ASME Paper No. GT2015-43127.
[24] Hurle, I., Price, R., Sugden, T., and Thomas, A., 1968, "Sound Emission From Open Turbulent Premixed Flames," Proc. R. Soc. A, **303**(1475), pp. 409–427.
[25] Paschereit, C. O., and Polifke, W., 1998, "Investigation of the Thermoacoustic Characteristics of a Lean Premixed Gas Turbine Burner," ASME Paper No. 98-GT-582.
[26] Fischer, A., Hirsch, C., and Sattelmayer, T., 2006, "Comparison of Multi-Microphone Transfer Matrix Measurements With Acoustic Network Models of Swirl Burners," J. Sound Vib., **298**(1–2), pp. 73–83.
[27] Rienstra, S., and Hirschberg, A., 2016, *An Introduction to Acoustics*, Eindhoven University of Technology, Eindhoven, The Netherlands.
[28] Lieuwen, T., 2005, *Unsteady Combustor Physics*, Cambridge University Press, Cambridge, UK.
[29] Howe, M. S., 1998, *Acoustics of Fluid-Structure Interactions*, Cambridge University Press, Cambridge, UK.
[30] Palies, P., Durox, D., Schuller, T., and Candel, S., 2011, "Experimental Study on Effects of Swirler Geometry and Swirl Number on Flame Describing Functions," Combust. Sci. Technol., **183**(7), pp. 704–717.
[31] Lighthill, M. J., 1952, "On Sound Generated Aerodynamically," Proc. R. Soc. London A, **211**(1107), pp. 564–587.
[32] Howe, M. S., 1979, "On the Theory of Unsteady High Reynolds Number Flow Through a Circular Aperture," Proc. R. Soc. London A, **366**(1725), pp. 205–223.
[33] Ni, F., Miguel-Brebion, M., Nicoud, F., and Poinsot, T., 2017, "Accounting for Acoustic Damping in a Helmholtz Solver," AIAA J., **55**(4), pp. 1205–1220.